FRACTURE MECHANICS OF CORTICAL BONE AT THE MICROSCALE BY SRμCT IMAGING AND DIGITAL VOLUME CORRELATION

Marta Peña Fernández (1), Jakob Schwiedrzik (2), Alexander Bürki (3), Françoise Peyrin (4), Johann Michler (2), Philippe Zysset (3), Uwe Wolfram (1)

1. School of Engineering and Physical Science, Heriot-Watt University, UK; 2. EMPA, Swiss Federal Laboratories for Materials Science and Technology, Switzerland; 3. ARTORG Centre, University of Bern, Switzerland; 4. Université de Lyon, CNRS 5220, INSERM U1294, CREATIS, France

Introduction

The high resistance of bone to fracture originates from multiple toughening mechanisms that span several length scales [1]. Aging and disease lead to increased risk of bone fracture and it remains important to understand the mechanisms of crack growth in relation to these structural length scales to improve fracture prevention strategies. Here, we evaluate local fracture properties from full-field displacements in cortical bone tissue at the microscale. We combine *in situ* high-resolution synchrotron radiation micro-computed tomography (SRμCT) indentation and digital volume correlation (DVC) to quantify three-dimensional crack opening displacements and stress intensity factors along the crack front.

Materials and methods

Ovine cortical bone specimens (3 mm diameter, 4 mm length) were subjected to *in situ* step-wise indentation in beamline ID19 at ESRF using a custom-made microindenter equipped with a 30 μm high Berkovich tip. Specimens were loaded with three ~10 μm displacements steps and phase-contrast SRμCT images (0.67 μm voxel size) were acquired after mechanical relaxation. DVC was used to evaluate the full-field displacement distribution around indentation-induced cracks. Mode I, II and III crack opening displacements were obtained from the displacement difference on either side of the crack. We used a least-square regression to fit the crack opening displacement data to Williams [2] expansion of near crack-tip displacement from which we extracted the stress intensity factors in Mode I, II, and III (i.e., K_I, K_{II}, and K_{III}) along the crack front following [3], assuming an elastic modulus and Poisson's ratio of 20 GPa and 0.3, respectively [4].

Results

3D crack opening displacements under the indenter tip were obtained (Figure 1). Median opening (Mode I) at the crack mouth amounted to 1.93 μm, while only 0.54 μm at the crack tip. Shear displacement (Mode II) remained below 1.5 μm at the crack mouth and 0.7 μm at the tip. Out of plane motion (Mode III) was less than 0.5 μm and 0.1 μm at the crack mouth and tip, respectively. Similarly, Mode I stress intensity factors were larger than Mode II and III in all analysed cracks and vary along the crack front. K_I ranged between 0.28 MPam$^{0.5}$ and 2.96 MPam$^{0.5}$, whilst K_{II} ranged between 0.01 MPam$^{0.5}$ and 0.50 MPam$^{0.5}$, and K_{III} between K_{III} 0.02 MPam$^{0.5}$ and 0.37 MPam$^{0.5}$.

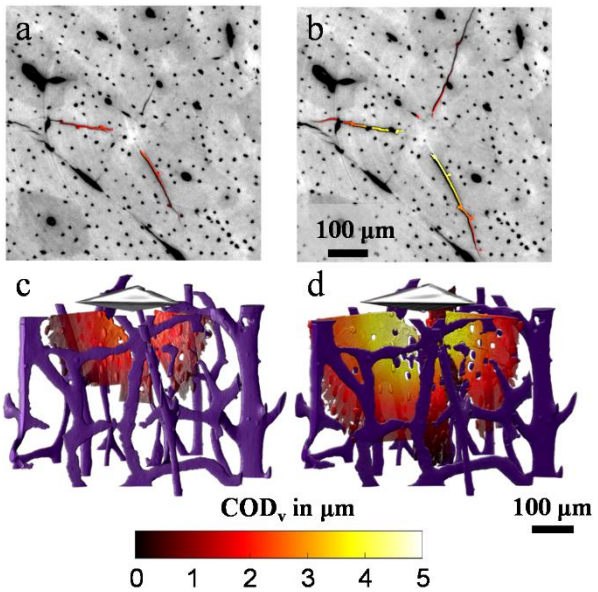

Figure 1: Mode I crack opening displacements (COD$_v$) under a Berkovich tip at (a, c) 20 μm and (b, d) 30 μm indentation depth. (a, b) 2D cross-sections 50 μm under the tip and (c, d) 3D renders showing segmented cracks.

Discussion

Crack opening displacements indicated a predominant Mode I fracture, as expected from the loading conditions. However, indentation loading with a Berkovich tip induced significant shear (Mode II). Variations of the stress intensity factors along the crack front emphasize the importance of a 3D characterization of the fracture toughness. K_I values were consistent with previous studies on a similar length scale, but lower than macroscale fracture testing [4]. Whilst we used here a linear-elastic fracture mechanics approach, future work will combine the experimental data with finite element analysis to account for the energy associated to plastic deformation [5]. Ultimately, this approach will allow us to explore bone failure in relation to microstructural changes due to aging or disease.

References

1. Launey et al, Annu Rev Mater Red, 40:25-53, 2010.
2. Williams, J Appl Mech, 28:78-82, 1960.
3. Limodin et al, Acta Mat, 57:4090-4101, 2009
4. Koester et al, Nat Mat, 7:672-677, 2008.
5. Shen et al, J Nuclear Mat, 563:153642, 2022.

Acknowledgements

Leverhulme Trust (RPG-2020-215) and AO Foundation (AO S-12-13W). Beam-time provided by ESRF (LTP MD431).